

# Energy Landscape of an Electron Hole in Hydrated DNA

Angelo Bongiorno

School of Chemistry & Biochemistry, Georgia Institute of Technology, Atlanta, Georgia 30332-0400

Received: March 3, 2008; Revised Manuscript Received: July 28, 2008

First-principles/molecular mechanics, force-field, and 1-D lattice model schemes are used to address the energy landscape of an electron hole in hydrated DNA. Force-field calculations are used to derive a statistical description of the electrostatic fluctuations in DNA yielded by the polar environment, and a periodic first-principles/molecular mechanics scheme is employed to calculate the hole energy at uniform DNA segments embedded in hydrated DNA double helices. The results are then mapped onto 1-D lattice models to address issues relevant to charge transfer in hydrated DNA. It is shown that the polar environment generates an intense dynamical energy disorder along the DNA strands, exhibiting exponential spatio-temporal correlations. The fluctuations of the polar environment lead to hole states localized over a few DNA bases and compete evenly with the DNA sequence to define the hole energy landscape. The spatial correlations of the environment-induced fluctuations are also shown to influence strongly the hole transfer dynamics in DNA.

## I. Introduction

Charge transfer in DNA is an important biological step involved in oxidative DNA damage<sup>1</sup> and DNA repair mechanisms.<sup>2</sup> Understanding this process is crucial not only for its biological relevance but also for the development of DNA-based devices.<sup>3</sup>

Biochemical experiments on charge transfer in DNA have mostly focused over the recent decades on the electron hole dynamics in DNA oligomers immersed in aqueous solution.<sup>4–16</sup> These studies have reported intervals of  $10^5$ – $10^{12}$  s<sup>−1</sup> and 0.1–2.0 Å<sup>−1</sup> for the charge transfer rate and the distance-decay constant, respectively, indicating that hole dynamics occurs on multiple time scales and relates nontrivially to the DNA attributes. The challenging interpretation of this experimental information<sup>4–16</sup> has centered around three major issues. First, the charge transfer mechanism: bridge-assisted tunneling steps, multistep hole hopping,<sup>17–23</sup> or phonon-assisted polaron hopping.<sup>13</sup> Second, the spatial extension of an electron hole in DNA: strongly localized on one single DNA base<sup>24,25</sup> vs delocalization over extended DNA domains.<sup>25,26</sup> Third, the molecular processes triggering and/or limiting the charge transfer motion: proton transfer processes,<sup>27–30</sup> in contact DNA–Na<sup>+</sup> states,<sup>31,32</sup> base pair motion,<sup>33</sup> and DNA domain conformational distortions.<sup>34</sup> These issues remain still to date unsolved, and in spite of recent progress,<sup>25–34</sup> the description of charge transfer phenomena in hydrated DNA relies again mainly on phenomenological theories.<sup>17–23</sup>

A variety of computational schemes have been utilized to address issues relevant to charge transfer in DNA.<sup>35–44</sup> 1-D lattice tight-binding calculations have been used to investigate the role of sequence, DNA dynamics, and base pairing on the charge transport properties of DNA.<sup>35–39</sup> First-principles schemes have been employed to address the electronic properties of an electron hole at selected DNA systems<sup>40–42</sup> or to calculate intra- and interstrand base–base electronic couplings.<sup>43,44</sup> In these studies, the aqueous environment has been ill-represented or entirely neglected. Recently, a hybrid semiempirical first-principles/molecular mechanics scheme has been used to address the reaction free energy of hole transfer steps between guanine and adenine bases in a DNA oligomer of finite length in aqueous

solution.<sup>45</sup> This study highlighted the importance of solvent fluctuations on charge transfer in DNA.<sup>45</sup>

The present study addresses at the molecular level issues pertaining to charge transfer processes in DNA. In particular, we investigated the effect of the polar environment and DNA sequence on the energy landscape of an electron hole in hydrated DNA. We considered a set of linear, periodically repeated hydrated DNA duplexes composed of regular stacks of base pairs. Then, we designed a set of force-field and periodic first-principles/molecular mechanics calculations with the scope of reducing the complexity of the electron hole energy landscape to single base information to be transferred onto 1-D lattice models. In this study we show that the electron hole energy is controlled in equal measure by the polar environment and the DNA composition. The fluctuating polar environment generates along the DNA strands an intense dynamical energy disorder, exhibiting well-defined exponential spatio-temporal correlations. We also show that the hole energy fluctuations generated by the polar environment yield hole states localized over a few DNA bases and that spatial correlations are connected to the hole transfer dynamics in hydrated DNA.

## II. Methods and Simulations

**A. Computational Schemes.** The first-principles (QM) scheme is based on a plane-wave density-functional approach<sup>46</sup> formulated to describe either periodic or finite systems.<sup>47</sup> Only valence wave functions are treated explicitly, and core–valence interactions are described through the use of norm-conserving<sup>48</sup> (H, P, and Na atoms) or ultrasoft<sup>49</sup> pseudopotentials (C, N, and O atoms). The exchange and correlation energy is calculated within a spin-polarized generalized gradient approximation.<sup>50</sup> In this study, we used a plane-wave energy cutoff of 30 Ry.

The molecular mechanics (MM) scheme utilizes the Amber force field for the description of nucleic acids and Na<sup>+</sup> counterions.<sup>51,52</sup> H<sub>2</sub>O molecules are treated according to the TIP3P model potential.<sup>53,54</sup> The MM scheme is used in conjunction with a molecular dynamics (MD) approach for statistical thermodynamics studies of DNA systems in aqueous solution. In case of periodic systems, the Coulomb interactions are evaluated through the use of the Ewald sums. Constant-

temperature MD simulations are performed by coupling the system to a Nosé-Hoover thermostat.<sup>55</sup> In this study, we used a thermostat relaxation time of about 0.1 ps.

The hybrid first-principles/molecular mechanics (QM/MM) methodology is obtained by merging the previous QM and MM schemes, as described in ref 56. In this study, we adopted a novel formulation of the QM/MM scheme allowing for the description of periodic systems. In this periodic QM/MM formulation, the MM and QM schemes share the same real and reciprocal space, and the electrostatic interactions between the MM and QM regions are calculated exactly by using the Ewald method. Besides the hybrid nature of the scheme, no additional approximations are included in our periodic QM/MM scheme.

1-D lattice models are used to represent the energy landscape of an electron hole in hydrated DNA. We adopted the following lattice Hamiltonian:

$$\mathcal{H} = \sum_i \varepsilon_i c_i^\dagger c_i - t(c_i^\dagger c_{i+1} + c_i c_{i+1}^\dagger) \quad (1)$$

where  $c_i^\dagger$  ( $c_i$ ) is the creation (annihilation) operator,  $\varepsilon_i$  is the electron hole energy at the lattice site  $i$ , and  $t$  is the interbase electronic coupling. In this study, lattice sites are coupled electronically to only their first next neighbors and  $t$  is assumed to be a constant equal to 0.1 eV.<sup>43</sup> The lattice site energies,  $\varepsilon_i$ , are considered to account for both the nature of the DNA base and the polar environment. This information was derived from *first-principles*, through the use of MM and QM/MM simulations. For each eigenstate of eq 1, the hole localization length is defined as the inverse participation ratio.<sup>57</sup>

**B. MM and QM/MM Simulations.** We used MM molecular dynamics simulations to model DNA duplexes in aqueous solution at 300 K. Our model systems consist of 10-base-pair B-DNA double helices aligned along the  $z$  axis in a periodic cell of  $36 \text{ \AA} \times 36 \text{ \AA} \times 33.8 \text{ \AA}$ , including 1189  $\text{H}_2\text{O}$  molecules and 20  $\text{Na}^+$  counterions. We considered four DNA sequences: two DNA double helices composed of a regular stack of guanine/cytosine (G/C) and adenine/thymine (A/T) base pairs and two other DNA duplexes including two GG/CC steps separated on both sides by three sequential A/T and T/A base pairs. In short, the sequence of the periodic DNA chains are  $-(\text{G})_{10}/-(\text{C})_{10}-$ ,  $-(\text{A})_{10}/-(\text{T})_{10}-$ ,  $-(\text{GGAAA})_2/-(\text{CCTTT})_2-$ , and  $-(\text{GGTTT})_2/-(\text{CCAAA})_2-$ . Each DNA system was evolved for  $\sim 2.6$  ns at 300 K, after an equilibration step of  $\sim 0.5$  ns. We note here that the results of the MM study showed little dependence on the DNA sequence, and for this reason, they are presented in section IIIA in their generality, without referring to the specific DNA systems.

We used the periodic QM/MM scheme to calculate the vertical ionization potential ( $E_v$ ) of uniform 10-base segments composed of G, A, C, and T bases embedded in a hydrated B-DNA duplex. For this purpose, we considered the periodic systems employed in the MM study consisting of uniform hydrated DNA duplexes composed of only G/C and A/T base pairs. To address the ionization process at a single 10-base DNA strand, QM/MM partitions were obtained by including one full periodic strand in the QM region, while the complementary strand, the  $\text{Na}^+$  counterions, and the  $\text{H}_2\text{O}$  molecules were all described through the MM scheme. This partition involves molecularly disconnected QM and MM regions, interacting only through nonbonded interactions.<sup>51,52</sup> A graphical representation of such a QM/MM partition is shown in Figure 1.

In the ionized state the periodic DNA systems include a positive charge which in our QM/MM calculations is neutralized

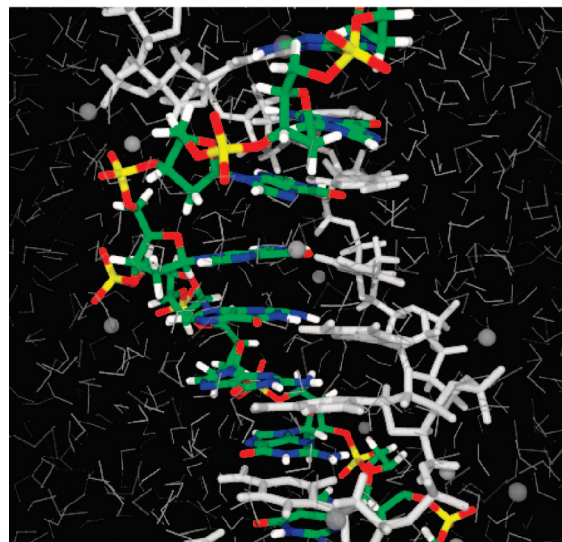


**Figure 1.** Ball and stick representation of a B-DNA double helix immersed in aqueous solution. Colors are used only for DNA strand described through the QM scheme in a periodic QM/MM calculation. Gray is used for the MM components: complementary strand, water environment, and  $\text{Na}^+$  counterions (balls).

**TABLE 1: Vertical ( $E_v$ ) and Adiabatic ( $E_a$ ) Ionization Potential (in eV) of Isolated DNA Bases in Vacuum<sup>a</sup>**

	$E_v$			$E_a$		
	QM	HL-QM	exp	QM	HL-QM	exp
G	7.8	8.1	8.0–8.3	7.5	7.6	7.7–7.8
A	8.1	8.4	8.3–8.5	7.9	8.1	7.8–8.5
C	8.6	8.7	8.8–9.0	8.5	8.6	8.4–8.7
T	8.8	9.1	9.0–9.2	8.6	8.8	8.8–8.9

<sup>a</sup> Energy values obtained by using our QM scheme are compared to both high-level quantum chemical ab initio (HL-QM) and experimental data, both taken from ref 59.

by a uniform background.<sup>58</sup> The energy correction to  $E_v$  arising from the spurious interaction of the positive excess charge and the uniform background does not exceed 0.1 eV.<sup>58</sup>

**C. QM and QM/MM Preliminary Calculations.** To assess the accuracy of our QM scheme, we calculated the vertical ( $E_v$ ) and adiabatic ( $E_a$ ) ionization potentials of isolated DNA bases in vacuum, and we compared our QM results to both experimental and high-level quantum chemical ab initio values<sup>59</sup> (Table 1). The ionization potentials were obtained as energy difference between the neutral and ionized DNA base.  $E_a$  accounts for the ionic relaxations of the ionized base, while  $E_v$  is derived by preserving the geometry of the neutral base. The comparison showed that our QM results agree well with both theoretical and experimental data (Table 1). In particular, Table 1 shows that our QM scheme describes accurately, at the level of quantum chemical ab initio methods, the relative energy values of an electron hole at DNA bases, while the absolute values exhibit systematic deviations of about 0.2 eV. This error arises from self-interaction, spin contamination, and thermal effects.

To validate the QM/MM and MM schemes used in the present study, we addressed the ionization process at selected oligomers by using both the QM and QM/MM schemes. We considered one 2-base-pair and two 4-base-pair B-form DNA duplexes including sugar–phosphate backbones and  $\text{Na}^+$  counterions. The oligomer sequences are reported in Table 2. QM/MM partitions were obtained by assigning one full strand to the QM scheme and the complementary strand plus  $\text{Na}^+$  counterions to the MM

**TABLE 2:**  $E_v$  and  $E_a$  (in eV) and Hole Population Fractions (in %) for Selected B-DNA Duplexes<sup>a</sup>

oligomer	$E_v$	$E_a$	3'-side	G	G	5'-side
GG/CC	5.5	5.0		43	57	
GG/CC	5.5	5.1		42	58	
AGGA/TCCT	4.3	3.8	4	42	53	1
AGGA/TCCT	4.4	3.7	3	43	52	1
TGGT/ACCA	4.4	3.8	1	44	55	0
TGGT/ACCA	4.5	3.9	1	42	54	1

<sup>a</sup> In the first column, the slash symbol separates complementary strands and bold (normal) letters are used to indicate bases in the MM (QM) region. Hole population fractions are reported only for the strand including the GG doublet, from left to right following strand direction.

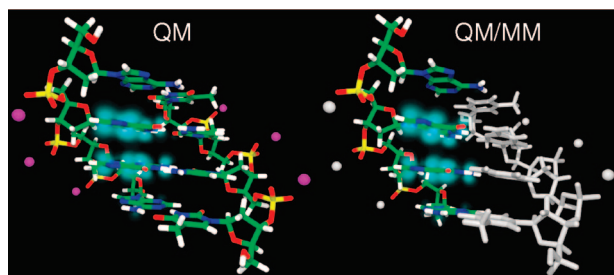


**Figure 2.** Ball and stick representations of an ionized 4-base-pair B-DNA oligomer, described through the QM (left) and QM/MM (right) scheme.  $\text{Na}^+$  ions were located along the bisectors of the O1P–P–O2P groups at a distance of 2.7 Å from the P atoms and held fixed during the QM and QM/MM geometrical optimizations. Colors and gray are used for the QM and MM regions, respectively. The electron spin density (hole) is also shown in light blue.

region (Figure 2). Thus, for each oligomer we adopted both the QM and QM/MM scheme to calculate  $E_v$ ,  $E_a$ , and the hole population fractions at the ionized DNA strand. Hole fractions were obtained through the integration of the electron spin density over the real space grid, partitioned by assigning each grid point to the closest nucleobase.

The results of the QM and QM/MM calculations are reported in Table 2. We note that  $E_v$  of the 2-base-pair DNA oligomer is in excellent agreement with the value reported in ref 60. Furthermore, in accord with both experiment<sup>61,62</sup> and theory,<sup>60,62</sup> our results show that both pairing and stacking contribute to decrease the ionization potential of DNA oligomers. As for the comparison of the QM and QM/MM results, Table 2 shows that QM and QM/MM hole energies and fractions differ by at most 0.15 eV and 2%, respectively. This agreement stems from two separate qualities of our QM/MM calculations, that is, the MM force field, which describes accurately the electrostatic field in DNA, and the partition of the DNA duplexes (in molecularly disconnected QM and MM regions including one DNA strand each), which leads to adequate treatments of an electron hole at a DNA strand.

### III. Results and Discussion

**A. Electrostatic Fluctuations in DNA.** We investigated at first the effect of the polar environment on the hole energy in DNA. To this end, we monitored the temporal and spatial progression of the electrostatic potential in DNA generated by using a MM molecular dynamics approach (section IIA). To exclude secondary structure and end effects, we considered a set of infinite, periodically repeated DNA duplexes composed of a linear stack of base pairs and immersed in aqueous solution (section IIB). Furthermore, to reduce confidently the complexity of the electrostatic potential in DNA to statistical single-base

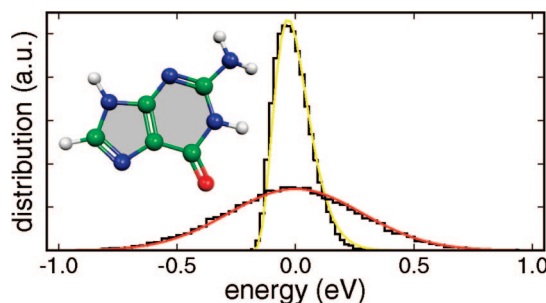


**Figure 3.** Distribution of the mean value (broad Gaussian-like) and rms deviation (peaked Gamma-like) of the electrostatic potential across the base plane of a G base embedded in hydrated DNA. Black histograms correspond to the distributions extracted from the MD simulations, while colored lines are functional fit. Distributions are plotted by referring the energy scale to the respective average values. A ball-and-stick representation of a G base is shown. The electrostatic potential is sampled uniformly in the interior of the aromatic rings (gray regions).

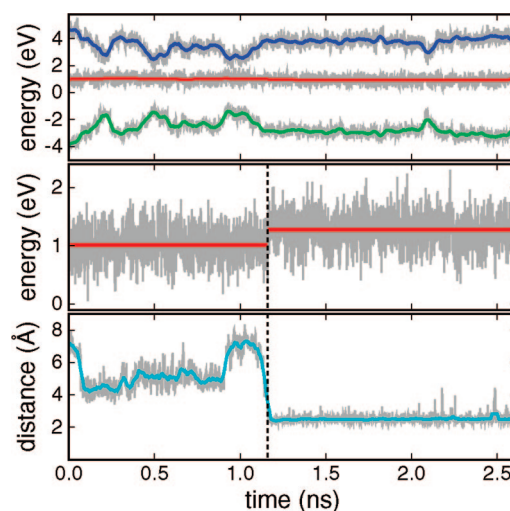


**Figure 4.** Top and middle panels: potential energy level vs time at a G base embedded in hydrated DNA. Top panel: the contributions arising from liquid water (upper line) and the DNA chain plus  $\text{Na}^+$  ions (bottom line) are shown separately. Bottom panel: minimum distance vs time between the atoms of the G base and the  $\text{Na}^+$  counterions. The vertical dashed line indicates the transition of a  $\text{Na}^+$  counterion from a free, not in contact state to a bound, in contact configuration with the G base. Gray lines are extracted from MD simulations, while the colored lines are guides to the eye.

information, we selected several DNA double helices including either no or little sequence disorder (section IIB). Hence, the monitoring operation was performed at intervals of 0.1 ps along the MD trajectories by sampling the electrostatic potential uniformly in the interior of the heterocyclic aromatic rings of each base along the DNA strands. From this sampling, we retained only the mean value and rms deviation of the electrostatic potential at the DNA bases (Figure 3).

At a DNA base, the rms deviation of the electrostatic potential reflects the inhomogeneity of the local surroundings, caused by base stacking, base pairing, and the nonuniform exposure to the aqueous solution. The analysis of the MD trajectories showed that the rms deviations are distributed narrowly around a value of  $\sim 0.25$  eV with an energy width of  $\sim 0.07$  eV. This width is four/five times smaller than the standard deviations of the mean values of the electrostatic potential at the DNA bases (Figure 3). For this reason, as a first approximation in this study we neglected the details of the electrostatic potential across the base plane, and we focused only on the statistical features of



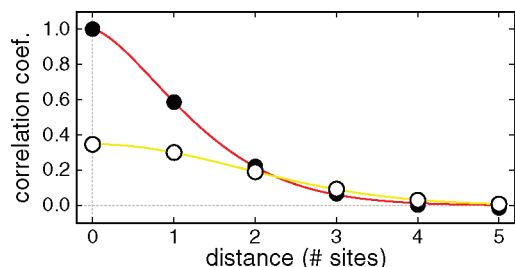


**Figure 5.** Interstrand (empty circles, yellow line) and intrastrand (discs, red line) spatial correlations of the potential energy level fluctuations at the DNA bases. Discs and empty circles are derived from MD simulations, while colored lines are functional fits (eq 2). Distance is in interbase spacing units.

the corresponding mean values, to which hereafter we will refer to as *potential energy level*.

The MD simulations showed that the potential energy levels at G, A, C, and T bases along the DNA strands are distributed normally around the values 1.0, 1.1, 0.7, and 0.9 eV, respectively. The standard deviations of the normal distributions are 0.30, 0.27, 0.30, and 0.25 eV at the G, A, C, and T bases, respectively. The mean energies of the potential energy levels correspond to a measure of the solvation free energy of an electron hole at the DNA bases. The MM simulations showed that the hole solvation free energy remains constant on the nanosecond time scale, raising suddenly by  $\sim 0.3$  eV at G bases entering in direct contact with a  $\text{Na}^+$  counterion (Figure 4). This result is in agreement with recent *ab initio* calculations.<sup>31,32</sup>

The deviations of the potential energy levels exhibit well-defined temporal and both intra- and interstrand spatial correlations.<sup>45</sup> Temporal correlations decay exponentially with a time constant of 5.3 ps, while spatial correlations follow a nontrivial exponential decaying (Figure 5). In particular, we found that the correlation coefficient,  $\gamma$ , of the deviations,  $\Delta E$ , of the potential energy level at two DNA bases separated by  $n$  interbase spacing units is well reproduced by the following exponential function:

$$\gamma_n = \left\langle \frac{\Delta E_i \Delta E_{i+n}}{\sigma_i \sigma_{i+n}} \right\rangle_{i,t} = C_0 \exp \left\{ -\left( \frac{n}{\lambda} \right)^\beta \right\} \quad (2)$$

where  $\sigma_i$  corresponds to the standard energy deviation of the energy level at the base  $i$ , the average  $\langle \dots \rangle_{i,t}$  is taken over both the base index and time, and  $C_0$  and  $\beta$  are equal to 1.0 and 1.5 and 0.35 and 2 in case of intra- and interstrand correlations, respectively. The correlation length,  $\lambda$ , in eq 2 is equal to 1.5 ( $\sim 5$  Å) and 2.6 ( $\sim 8.8$  Å) base spacing units, in the case of intra- and interstrand correlations, respectively. We highlight that in the case of interstrand spatial correlations  $C_0$  gives the correlation coefficient between the potential energy level deviations of two paired cDNA bases (Figure 5).

To elucidate the nature of the spatio-temporal correlations, we carried out a separate MM study. This study showed that the correlations of the potential energy level fluctuations along the DNA strands stem from the structural and dielectric properties of the hydration layers surrounding the DNA chain. The results of this study lie outside the scope of this work and hence will be presented elsewhere.

**B. Hole Energy at DNA Bases in Hydrated DNA.** To account for the role of DNA sequence and, thus, complete the base-level description of the hole energy landscape in hydrated DNA, we used our periodic hybrid QM/MM scheme (section

IIA). In particular, we calculated the vertical ionization potential ( $E_v$ ) of uniform DNA strands composed of only G, A, C, or T bases inserted in periodic 10-base-pairs B-DNA duplexes immersed in aqueous solution, as described in section IIB. Ten thermal configurations were extracted at random from the MD trajectory of the uniform DNA duplex composed of G/C and A/T base-pairs, respectively. Each thermal configuration was used twice, in order to calculate alternatively  $E_v$  at the two cDNA strands. In these QM/MM calculations, the QM scheme was used to describe one full periodic DNA strand, while the rest of the system was treated by the MM scheme (Figure 1). We note that the calculated  $E_v$ s account for stacking, pairing, and hydration effects and exclude polaron effects.

The QM/MM calculations yielded  $E_v$ s centered around 6.1, 6.6, 6.8, and 7.1 eV for segments of G, A, C, and T bases, respectively. In all cases, the  $E_v$ s are distributed with a rms deviation of  $\sim 0.2$  eV, suggesting that the error on the mean values is of the order of 0.06 eV, that is, 1% of their absolute values. These results are consistent with photoionization experiments of hydrated DNA poly nucleotides, reporting a one-photon ionization threshold of  $\sim 5.9$  eV.<sup>63,64</sup>

Overall, the QM/MM study showed that stacking, pairing, and hydration effects contribute to decrease the hole energy by  $\sim 1.7$  eV with respect to the value at the single isolated bases in vacuum (Table 1). The energy order is preserved, and as expected, the lowest  $E_v$  is found at G segments, while at DNA segments composed of A, C, and T bases,  $E_v$  raises by 0.5, 0.7, and 1.0 eV, respectively. These results show that DNA sequence and polar environment yield comparable levels of energy disorder along the DNA strands.

In the context of a 1-D lattice representation of the hole energy landscape in DNA (section IIA), the QM/MM mean values of  $E_v$  at the G, A, C, and T segments can be corresponded to the reference hole energy at the G, A, C, and T lattice sites, respectively. This correspondence is valid under the assumption of a uniform and constant intrabase electronic coupling (eq 1).

**C. Hole Localization Length and Transfer Dynamics.** To highlight the implications of our results, we addressed the effect of the polar environment on the hole energy, localization length, and transfer dynamics by using 1-D lattice models (section IIA). In particular, we modeled the case of an electron hole in a single DNA strand. To account for both strand composition and polar environment, lattice site energies were assigned according to normal distributions whose mean values and standard deviations were derived from the QM/MM and MM studies, respectively. Furthermore, energy deviations were mapped across the lattice model either at random or according to the correlation function of the intrastrand energy fluctuations in eq 2. The following results have been obtained by averaging over the energy disorder yielded by the polar environment.

We first considered a uniform 10-site lattice model, mimicking the geometry of the DNA systems employed in the QM/MM study. Tight-binding calculations showed that the lowest-energy states are distributed around an energy value 0.5 eV below the mean lattice site energy, with a rms deviation of 0.2 eV. These results show that the hole solvation energy of  $\sim 1.7$  eV at 10-base uniform DNA segments in hydrated DNA can be splitted in three separate contributions, arising respectively from solvation effects, which amount to  $\sim 1.0$  eV, an interbase electronic coupling of about  $2t = 0.2$  eV, and the environment-induced energy disorder, which accounts for the remaining 0.3–0.5 eV.

We then considered the limit case of long, nearly infinite uniform DNA strands. Our tight-binding calculations showed

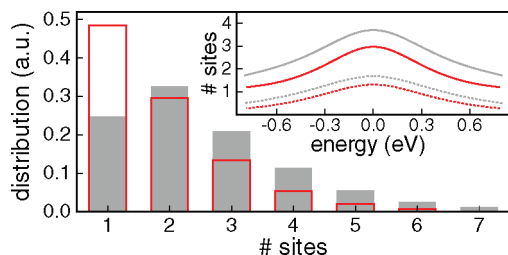


**Figure 6.** Distribution of hole localization lengths in long, uniform DNA strands obtained from 1-D lattice model calculations. Inset: mean value (full lines) and rms deviation (dotted lines) of the localization length vs hole energy. Gray (red) is used to plot the results derived assuming a spatial correlated (uncorrelated) dynamic energy disorder.

that the total density of states is equal to the single-site normal distribution of environment-induced energy deviations and that hole states extend over  $2.3 \pm 1.1$  and  $3.1 \pm 1.5$  lattice sites in case of uncorrelated and correlated energy deviations, respectively (Figure 7). In both cases, over the entire energy spectrum the mean localization length does not exceed 4 base units and tends to unity at large negative and positive hole energy values (Figure 7, inset). We note that the occurrence of spatial correlations affects marginally the hole localization length, as it increases by at maximum 1 base unit with respect to the case of uncorrelated energy deviations (Figure 7).

At last, we addressed the connection between spatial correlations and hole transfer dynamics. For this purpose we considered 1-D lattice representations of DNA strands composed of repeating GX steps, with X equal to G, A, C, or T. Then, we performed lattice model statistical calculations to estimate  $P_{GX}$ , the probability that at a GX step the G site exceeds in energy the neighboring X site. This quantity corresponds to a measure of the strength of the polar environment to drive  $G \rightarrow X$  hole transfer steps. When X is equal to G, the case of a uniform lattice model is recovered and  $P_{GX}$  acquires the obvious value of 0.5 (Figure 7). We note that, in the context of a kinetic treatment of charge transfer in DNA,<sup>17</sup>  $P_{GX}$  may be corresponded to the Franck–Condon factor of the forward  $G \rightarrow X$  hole hopping rate.<sup>17</sup>

Our lattice model calculations showed that in absence of spatial correlations  $P_{GX}$  assumes in all cases non-negligible values. The occurrence of spatial correlations, however, decreases  $P_{GX}$  importantly. For strands of repeating GC or GT steps, for instance,  $P_{GX}$  drops by 1 and 2 orders of magnitude, respectively (Figure 7). This result shows that the spatial correlations of the environment-induced energy disorder influence significantly the hole transfer dynamics in DNA. In particular, Figure 7 suggests that spatial correlations may raise rapidly the importance of both bridge-assisted tunneling processes and interstrand transfer steps with the level of the DNA compositional disorder.

#### IV. Conclusions

In this study we used MM, QM/MM, and 1-D lattice model calculations to address the energy of an electron hole in hydrated DNA. MM molecular dynamics simulations were used to derive a statistical description of the environment-induced hole energy fluctuations at the single DNA base, while a periodic QM/MM scheme was employed to estimate the hole solvation free energy at G, A, C, and T bases embedded in hydrated DNA double helices. Then, the MM and QM/MM results were transferred onto 1-D lattice models to infer information on the energetics, localization length, and transfer dynamics of an electron hole

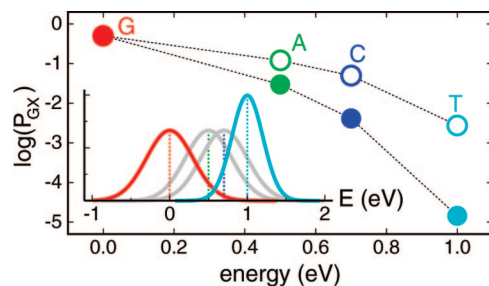


**Figure 7.** Logarithm of  $P_{GX}$  (see text), with X equal to G (red), A (green), C (blue), and T (cyan). Filled (open) symbols connected by a dotted line refer to 1-D lattice calculations including spatial correlated (uncorrelated) potential energy level fluctuations. Inset: distribution of the potential energy levels at G, A, C, and T bases embedded in hydrated DNA. Gaussian distributions are centered around the mean  $E_v$ s obtained from QM/MM calculations. The mean  $E_v$  at G is set to zero. For clarity, the central distributions are shown in gray.

in DNA. This study is based on two main approximations. First, interbase electronic couplings are assumed to be equal to a constant. Second, polaron effects are neglected. Both are not expected to alter the significance of our results.

This study shows that the polar environment generates an intense dynamical energy disorder along the DNA strands, exhibiting exponential spatio-temporal correlations. In uniform DNA strands, these energy fluctuations are capable to yield hole states localized over a few DNA bases. Our study shows, in addition, that the polar environment and DNA sequence yield along a DNA strand comparable levels of energy disorder and that the ability of the polar environment to drive the hole transfer motion is reduced significantly by the occurrence of spatial correlations.

**Acknowledgment.** We acknowledge useful discussions with J.-L. Brédas and V. Coropceanu. Computations were performed at the Center for Computational Molecular Science & Technology, at the Georgia Institute of Technology.

#### References and Notes

- (1) Steenken, S. *Chem. Rev.* **1989**, *89*, 503–520.
- (2) Park, H.; Kim, S.; Sancar, A. *Science* **1995**, *268*, 1866–1872.
- (3) Porath, D.; Cuniberti, G.; Felice, R. D. *Top. Curr. Chem.* **2004**, *237*, 183–227.
- (4) Barton, J.; Kumar, C.; Turro, N. *J. Am. Chem. Soc.* **1986**, *108*, 6391–6393.
- (5) Brun, A.; Harriman, A. *J. Am. Chem. Soc.* **1992**, *114*, 3656–3660.
- (6) Murphy, C.; Arkin, M.; Jenkins, Y.; Ghatlia, N.; Bossmann, S.; Turro, N.; Barton, J. *Science* **1993**, *262*, 1025–1029.
- (7) Gasper, S.; Schuster, G. *J. Am. Chem. Soc.* **1997**, *119*, 12762–12771.
- (8) Lewis, F.; Wu, T.; Zhang, Y.; Letsinger, R.; Greenfield, S.; Wasielewski, M. *Science* **1997**, *277*, 673–676.
- (9) Fukui, K.; Tanaka, K. *Angew. Chem., Int. Ed.* **1998**, *37*, 158–161.
- (10) Meggers, E.; Michel-Beyerle, M.; Giese, B. *J. Am. Chem. Soc.* **1998**, *120*, 12950–12955.
- (11) Meggers, E.; Kusch, D.; Wille, U.; Giese, B. *Angew. Chem., Int. Ed.* **1998**, *37*, 460–462.
- (12) Kelley, S.; Barton, J. *Science* **1999**, *283*, 375–381.
- (13) Henderson, P.; Jones, D.; Hampikian, G.; Kan, Y.; Schuster, G. *Proc. Natl. Acad. Sci. U.S.A.* **1999**, *96*, 8353–8358.
- (14) Wan, C.; Fiebig, T.; Kelley, S.; Treadway, C.; Barton, J.; Zewail, A. *Proc. Natl. Acad. Sci. U.S.A.* **1999**, *96*, 6014–6019.
- (15) Williams, T.; Odom, D.; Barton, J. *J. Am. Chem. Soc.* **2000**, *122*, 9048–9049.
- (16) Lewis, F.; Liu, X.; Liu, J.; Miller, S.; Hayes, R.; Wasielewski, M. *Nature (London)* **2000**, *406*, 51–53.
- (17) Jortner, J.; Bixon, M.; Langenbacher, T.; Michel-Beyerle, M. *Proc. Natl. Acad. Sci. U.S.A.* **1998**, *95*, 12759–12765.
- (18) Bixon, M.; Giese, B.; Wessely, S.; Langenbacher, T.; Michel-Beyerle, M.; Jortner, J. *Proc. Natl. Acad. Sci. U.S.A.* **1999**, *96*, 11713–11716.

- (19) Bixon, M.; Jortner, J. *J. Phys. Chem. B* **2000**, *104*, 3906–3913.
- (20) Bixon, M.; Jortner, J. *J. Am. Chem. Soc.* **2001**, *123*, 12556–12567.
- (21) Giese, B.; Wessely, S.; Spormann, M.; Lindemann, U.; Meggers, E.; Michel-Beyerle, M. *Angew. Chem., Int. Ed.* **1999**, *38*, 996–998.
- (22) Giese, B. *Acc. Chem. Res.* **2000**, *33*, 631–636.
- (23) Giese, B.; Amaudrut, J.; Köhler, A.-K.; Spormann, M.; Wessely, S. *Nature (London)* **2001**, *412*, 318–320.
- (24) Voityuk, A. *J. Chem. Phys.* **2005**, *122*, 204904.
- (25) Conwell, E. *Proc. Natl. Acad. Sci. U.S.A.* **2005**, *102*, 8795–8799.
- (26) Shao, F.; Augustyn, K.; Barton, J. *Proc. Natl. Acad. Sci. U.S.A.* **2004**, *101*, 17914–17919.
- (27) Giese, B.; Wessely, S. *Chem. Commun.* **2001**, *2001*, 2108–2109.
- (28) Shafirovich, V.; Dourandin, A.; Geacintov, N. *J. Phys. Chem. B* **2001**, *105*, 8431–8435.
- (29) Gervasio, F.; Laio, A.; Parrinello, M.; Boero, M. *Phys. Rev. Lett.* **2005**, *94*, 158103.
- (30) Gervasio, F.; Boero, M.; Parrinello, M. *Angew. Chem., Int. Ed.* **2006**, *45*, 5606–5609.
- (31) Barnett, R.; Cleveland, C.; Joy, A.; Landman, U.; Schuster, G. *Science* **2001**, *294*, 567–571.
- (32) Barnett, R.; Cleveland, C.; Landman, U.; Boone, E.; Kanvah, S.; Schuster, G. *J. Phys. Chem. A* **2003**, *107*, 3525–3537.
- (33) Valis, L.; Wang, Q.; Raytchev, M.; Buchvaron, I.; Wagenknecht, H.-A.; Fiebig, T. *Proc. Natl. Acad. Sci. U.S.A.* **2006**, *103*, 10192–10195.
- (34) Shao, F.; Augustyn, K.; Barton, J. *J. Am. Chem. Soc.* **2005**, *127*, 17445–17452.
- (35) Grozema, F.; Berlin, Y.; Siebbeles, L. *J. Am. Chem. Soc.* **2000**, *122*, 10903–10909.
- (36) Bruinsma, R.; Grüner, G.; D’Orsogna, M.; Rudnik, J. *Phys. Rev. Lett.* **2000**, *85*, 4393–4396.
- (37) Grozema, F.; Siebbeles, L.; Berlin, Y.; Ratner, M. *ChemPhysChem* **2002**, *6*, 536–539.
- (38) Basko, D.; Conwell, E. *Phys. Rev. Lett.* **2002**, *88*, 098102.
- (39) Wang, X.; Chakraborty, T. *Phys. Rev. Lett.* **2006**, *97*, 106602.
- (40) Lewis, J. P.; Cheatham, T. E., III.; Starikov, E. B.; Wang, H.; Sankey, O. F. *J. Phys. Chem. B* **2003**, *107*, 2581–2587.
- (41) Alexandre, S.; Artacho, E.; Soler, J.; Chacham, H. *Phys. Rev. Lett.* **2003**, *91*, 108105.
- (42) Artacho, E.; Machado, M.; Sánchez-Portal, D.; Ordejón, P.; Soler, J. *Mol. Phys.* **2003**, *101*, 1587–1594.
- (43) Voityuk, A.; Jortner, J.; Bixon, M.; Rösch, N. *J. Chem. Phys.* **2001**, *114*, 5614–5620.
- (44) Mehrez, H.; Anantram, M. *Phys. Rev. B* **2005**, *71*, 115405.
- (45) Voityuk, A.; Siri Wong, K.; Rösch, N. *Angew. Chem., Int. Ed.* **2004**, *43*, 624–627.
- (46) Laasonen, K.; Pasquarello, A.; Car, R.; Lee, C.; Vanderbilt, D. *Phys. Rev. B* **1993**, *47*, 10142–10153.
- (47) Barnett, R.; Landman, U. *Phys. Rev. B* **1993**, *48*, 2081–2096.
- (48) Troullier, N.; Martins, J. *Phys. Rev. B* **1991**, *43*, 1993–2006.
- (49) Vanderbilt, D. *Phys. Rev. B* **1990**, *41*, 7892–7895.
- (50) Perdew, J.; Burke, K.; Ernzerhof, M. *Phys. Rev. Lett.* **1996**, *77*, 3865–3868.
- (51) Weiner, S.; Kollmann, P.; Nguyen, D.; Case, D. *J. Comput. Chem.* **1986**, *7*, 230–252.
- (52) Cornell, W.; Cieplak, P.; Bayly, C.; Gould, I.; Merz, K.; Ferguson, D.; Spellmeyer, D. C.; Fox, T.; Caldwell, J.; Kollman, P. *J. Am. Chem. Soc.* **1995**, *117*, 5179–5197.
- (53) Jorgensen, W. *J. Am. Chem. Soc.* **1981**, *103*, 335–340.
- (54) Jorgensen, W.; Chandrasekhar, J.; Madura, J.; Impey, R.; Klein, M. *J. Chem. Phys.* **1983**, *79*, 926–935.
- (55) Hoover, W. *Phys. Rev. A* **1985**, *31*, 1695–1697.
- (56) Barnett, R.; Bongiorno, A.; Cleveland, C.; Joy, A.; Landman, U.; Schuster, G. *J. Am. Chem. Soc.* **2006**, *128*, 10795.
- (57) Thouless, D. *Phys. Rep.* **1974**, *13*, 93–142.
- (58) Makov, G.; Payne, M. *Phys. Rev. B* **1995**, *51*, 4014–4022.
- (59) Roca-Sanjuán, D.; Rubio, M.; Merchán, M.; Serrano-Andrés, L. *J. Chem. Phys.* **2006**, *125*, 084302.
- (60) Sugiyama, H.; Saito, I. *J. Am. Chem. Soc.* **1996**, *118*, 7063–7068.
- (61) Caruso, T.; Carotenuto, M.; Vasca, E.; Peluso, A. *J. Am. Chem. Soc.* **2005**, *127*, 15040–15041.
- (62) Kim, N.; Zhu, Q.; LeBreton, P. *J. Am. Chem. Soc.* **1999**, *121*, 11516–11530.
- (63) Nikogosyan, D. *Int. J. Radiat. Biol.* **1990**, *57*, 233–299.
- (64) Candeias, L.; O’Neill, P.; Jones, G.; Steenken, S. *Int. J. Radiat. Biol.* **1992**, *61*, 15–20.

JP801872E